Author/s:
Petty, SJ;Milligan, CJ;Todaro, M;Richards, KL;Kularathna, PK;Pagel, CN;French, CR;Hill-Yardin, EL;O'Brien, TJ;Wark, JD;Mackie, EJ;Petrou, S

Title:
The antiepileptic medications carbamazepine and phenytoin inhibit native sodium currents in murine osteoblasts

Date:
2016-09-01

Citation:
Petty, S. J., Milligan, C. J., Todaro, M., Richards, K. L., Kularathna, P. K., Pagel, C. N., French, C. R., Hill-Yardin, E. L., O'Brien, T. J., Wark, J. D., Mackie, E. J. & Petrou, S. (2016). The antiepileptic medications carbamazepine and phenytoin inhibit native sodium currents in murine osteoblasts. Epilepsia, 57 (9), pp.1398-1405. https://doi.org/10.1111/epi.13474.

Accepted Date : 22-Jun-2016

Article type : Full length original research paper



**Full-length Original Research Article**

# The Anti-epileptic Medications Carbamazepine and Phenytoin Inhibit Native Sodium Currents in Murine Osteoblasts

**Sandra J. Petty MBBS PhD * [1-5], Carol J. Milligan PhD * [2],** Marian Todaro PhD [1], Kay L. Richards PhD [2], Pamuditha K. Kularathna BVSc [6], Charles N. Pagel BSc, PhD [6], Chris R. French MBBS, PhD [1,3,5], Elisa L. Hill-Yardin PhD [7], Terence J. O'Brien MD [1,3,5], John D. Wark MBBS PhD [5,8], Eleanor J. Mackie BVSc Dr med vet [6], Steven Petrou PhD [2].

** Petty and Milligan equal first authorship*

Authors' affiliations

1. Melbourne Brain Centre at The Royal Melbourne Hospital, The Department of Medicine, The University of Melbourne, Parkville, VIC, Australia
2. The Florey Institute of Neuroscience and Mental Health, Parkville, VIC, Australia
3. Department of Neurology, The Royal Melbourne Hospital, Parkville, Vic, Australia
4. Academic Centre, Ormond College, Parkville, VIC, Australia
5. Department of Medicine, The Royal Melbourne Hospital, The University of Melbourne, Parkville, VIC, Australia.
6. Faculty of Veterinary and Agricultural Sciences, The University of Melbourne, Parkville, VIC, Australia
7. Department of Physiology, University of Melbourne, Parkville, VIC, Australia
8. Bone and Mineral Medicine, The Royal Melbourne Hospital, Parkville, VIC, Australia

Corresponding author: Dr. Sandra Petty

Corresponding author's address: Department of Medicine, 1st Floor, Kenneth Myer Building, The University of Melbourne, Parkville VIC Australia 3052.

Corresponding author's phone and fax: Telephone + 61 3 9035 6379

Corresponding author's e-mail address: pettys@unimelb.edu.au

Running title: *Carbamazepine, phenytoin and osteoblasts*

Number of words in summary: 205

Number of words in main text: 2970

Number of figures: 3

Number of tables: 1

**SUMMARY**

Objective: Fracture risk is a serious comorbidity in epilepsy and may relate to the use of anti-epileptic medications. Many anti-epileptic medications inhibit ion channel function and the expression of these channels in osteoblasts raises the question whether altered bone signaling increases bone fragility. We aimed to: (1) confirm the expression of voltage-activated sodium channels ($Na_V$) in mouse osteoblasts, and (2) investigate the action of carbamazepine and phenytoin on $Na_V$ channels.

Methods: Immunocytochemistry was performed on primary calvarial osteoblasts extracted from neonatal C57BL/6J mice and additional RNA sequencing (RNASeq) was included to confirm expression of $Na_V$. Whole cell patch clamp recordings were made to identify the native currents expressed and to assess the actions of carbamazepine (50 μM) or phenytoin (50 μM).

Results: $Na_V$ expression was demonstrated with immunocytochemistry, RNA sequencing and functionally with demonstration of robust tetrodotoxin-sensitive and voltage-activated inward currents. Application of carbamazepine or phenytoin resulted in significant inhibition of current amplitude: for carbamazepine 31.6 ± 5.9 % (n = 9; $p<0.001$), and for phenytoin 35.5 ± 6.9 %, (n = 7; $p<0.001$).

Significance: Mouse osteoblasts express $Na_V$, and native $Na_V$ currents are blocked by carbamazepine and phenytoin supporting our hypothesis that AEDs can directly influence osteoblast function and potentially impact on bone strength.

**KEYWORDS**

Epilepsy, Bone Health, Osteoblast, Voltage-gated Sodium Channel, Electrophysiology

**ABBREVIATIONS**

| | |
|---|---|
| αMEM | alpha Minimum Essential Media |
| AED | Anti-epileptic Drug |
| AP | Action Potentials |
| BMD | Bone Mineral Density |
| CBZ | carbamazepine |
| DMEM | Dulbecco's Modified Eagle's Medium |
| DMSO | Dimethyl sulfoxide |
| FBS | Foetal Bovine Serum |
| FPKM | fragments per kilobase of exon per million fragments mapped |
| $Na_V$ | voltage-gated sodium channel |
| PHT | phenytoin |
| TEA | tetraethylammonium |
| TTX | tetrodotoxin |

**INTRODUCTION**

Patients with epilepsy have at least doubled fracture risk [1]. A proportion of patients, particularly those who have taken long-term anti-epileptic drug therapy have reduced bone density [2-4]. Causes of these associations are not fully understood [1; 5], particularly whether there are direct bone side-effects of AEDs. Approximately 1% of the population requires AED treatment for epilepsy, often of prolonged duration [6], with important treatment benefits, but also a risk of long-term adverse health effects [2; 7; 8]. More widespread use of AEDs for newer indications including migraine, chronic pain and bipolar affective disorder increases the imperative to determine whether AEDs increase fracture risk and, if so, by what mechanism(s). A more complete understanding of the mechanism for impaired bone health in epilepsy should facilitate the development of safer medications.

Initially, effects of AEDs on vitamin D metabolism were proposed as the primary mechanism for bone disease [9]; however, use of non-inducer AEDs, that do not impact vitamin D metabolism, is also associated with bone disease [10; 11]. Furthermore, there is a poor relationship between bone fracture risk and circulating vitamin D metabolite levels [3]. AEDs have multiple mechanisms of action; however, they all impact neuronal cellular signalling to exert their effects. In similar fashion, AEDs may impact bone cell signalling that may underlie a decrease in bone strength. Ion channels are common targets of many AEDs and both osteoblasts and osteocytes express ion channels, including some voltage-gated ion channels [12-14]. Ion channels have been implicated in transducing bone stress and strain [15-17] critical for modeling and remodeling. While osteocytes are often considered the primary mechano-sensing cells in bone, osteoblasts also are capable of responding to mechanical stress [18]. Osteoblasts possess multiple ion channels, including hyper-polarisation and osmolarity-sensitive channels [19], and voltage-gated sodium ($Na_V$) channels [20]. Another study observed rapid effects of Vitamin D3 on voltage-activated L-Ca and Cl− channels in the osteoblastic ROS 17/2.8 cell line and primary osteoblasts, and proposed that this mechanism may contribute to Vitamin D's ability to promote osteoblast secretory function; $Na_V$ were not included in that study [21]. Electric coupling between both rat and guinea pig osteoblast-like cells was reported to be inhibited by up to 59% by CBZ and PHT and the membrane potential depolarised by approximately 40-45% following CBZ; however, specific effects of AEDs upon $Na_V$ were not assessed in that study. $Na_V$s have a long-established role in electrogenesis in neurons [22] and are also expressed in "non-excitable" cells, with a range of effector functions, including attenuating cellular motility and migration, and driving reverse calcium importing in Na/Ca exchange [23]. Traditionally, osteoblasts are considered "non-excitable" cells [23]; however, there are ion channels present in osteoblasts which allow action potentials to be fired [20]. The role of $Na_V$ in osteoblasts and effects of AEDs such as CBZ and PHT on $Na_V$ in osteoblasts require investigation. We chose to initially investigate the AEDs CBZ and PHT as they have been associated with reduced BMD [3; 7] and fractures [24-26]. In this study, we investigated CBZ and PHT effects on $Na_V$ using whole-cell patch-clamp recording in mouse osteoblasts to examine for a direct effect of these anti-epileptic medications on osteoblasts. Better identification of the mechanisms underlying increased fracture rate and changes in bone quality seen in association with epilepsy and its treatment will allow for improving the targeting of fracture prevention strategies in patients with epilepsy.

## MATERIALS AND METHODS

### Calvarial Digests and Cell Culture

Primary osteoblasts were isolated from calvariae of C57BL/6J neonatal mice utilizing a previously published sequential collagenase digest protocol [27] with minor modifications. Briefly, calvariae were incubated in fresh digestion buffer containing collagenase type 1 (140Units/mL) (Worthington Biochemical Corporation, Lakewood NJ, USA), 0.05% (w/v) trypsin (Invitrogen, Carlsbad, CA, USA), and 2.5 mM $CaCl_2$ in Dulbecco's PBS at 37 °C 6 times for 20 min. Primary calvarial mouse osteoblasts were then maintained in alpha Minimum Essential Media (αMEM) supplemented with 10% (v/v) FBS and gentamicin (50 μg/ml) (Gibco Life Technologies, Grand Island, NY, USA) in culture flasks (BD Falcon, San Diego, CA, USA). Medium was changed every 3 to 4 days and cells were maintained as subconfluent cultures in a humidified incubator with 5% $CO_2$ in air at 37 °C. Samples of the cultured cells were stained for Alkaline Phosphatase (Sigma-Aldrich, St Louis, MO, USA) to confirm osteoblastic characteristics, and cells from digests positive for Alkaline Phosphatase were included in the Patchliner experiments.

Ethics approvals were obtained from the Howard Florey Institute Animal Ethics Committee (project number 13-028-UM) and all experiments were conducted in accordance with the Australian NHMRC guidelines on the ethical use of animals in scientific research [28].

**RNASeq Analysis**

First passage cells were grown until subconfluent in DMEM containing L-glutamine (2 mM) and 10% FBS, then cultured in BRFF-HPC1 medium (Athena Enzyme Systems, Baltimore, MD, USA) containing 10% FBS for 48 hours. Total RNA was extracted from 3 individual osteoblast isolates. Libraries were prepared from total RNA (5 μg) using the TruSeq RNA v2 sample preparation protocol (Illumina, San Diego, CA, USA); 100 bp paired-end sequencing was conducted using the HiSeq 2000 platform (Illumina) at the Australian Genomics Research Facility (Parkville, Australia), according to the manufacturer's instructions. After filtering and trimming, reads were mapped to the mouse reference genome assembly GRCm38/mm10 using the program TopHat [29] prior to transcripts being assembled from the aligned reads, using the program Cufflinks [30]. Results were expressed as FPKM (fragments per kilobase of exon per million fragments mapped), and a threshold of 0.3 was applied to FPKM as per previously described heuristic techniques [31]; 95% confidence intervals for FPKM were calculated.

**Cell Staining and Microscopy**

Primary calvarial osteoblast culture samples were stained for alkaline phosphatase to confirm osteoblastic characteristics using a kit (Sigma-Aldrich, Cat# 86C-1KT). Immunocytochemistry was performed using rabbit anti-rat $Na_V$ (Panα) (1:500; Cat # S6936) and Alexa-488 –conjugated goat anti-rabbit Ig (1:300; Molecular Probes, Cat# A11034); nuclei were counterstained using DAPI 4',6-diamidino-2-phenylindole (0.33 μg /mL, Cat # D9542 Sigma-Aldrich, St Louis, MO, USA). Fluorescent images were acquired using an Olympus FV1000 confocal microscope with an Olympus 60 x oil objective (NA 1.35).

**Electrophysiological recordings**

Electrical recordings were conducted using the Patchliner® (Nanion Technologies, Munich, Germany) in the whole-cell configuration. Before recordings, cells were detached from culture flasks with Accutase Cell Detachment Solution

(Innovative Cell Technologies Inc., San Diego, CA, USA) and resuspended at a density of $1x10^6$ to $5x10^7$ per milliliter in 50% αMEM (without FBS) and 50% external recording solution v/v. The external recording solution comprised (mmol/L): 140 NaCl, 4 KCl, 1 $MgCl_2$, 2 $CaCl_2$, 5 D-glucose, 10 HEPES, 10 tetraethylammonium (pH 7.4 with NaOH). The osmolarity of this solution was 298 mOsm. The internal recording solution comprised (mmol/L): 50 CsCl, 10 NaCl, 60 CsF, 2 $MgCl_2$, 20 EGTA, 10 HEPES, 3 $Mg^{2+}$-adenosine 5'-triphosphate, 10 TEA (pH 7.2 with CsOH) and the osmolarity of this solution was 285 mOsm. Solutions were filtered using a 0.2 μm membrane filter (Minisart; Sartorius Stedim Biotech, Goettingen, Germany). Cells were kept in suspension by gentle automatic pipetting. Medium single-hole planar NPC-16 chips with an average resistance of ~2.5 MΩ were used. Pipette and whole cell capacitance were fully compensated and the series resistance compensation was set to 50 %. Recordings were acquired at 50 kHz with the low pass filter set to 3 kHz in PATCHMASTER (HEKA Instruments Inc., NY, USA) and performed at 27 °C. Offline analysis was performed using Microsoft Excel and GraphPad Prism 6 (Molecular Devices). Data are shown as means ± S.E.M. Leak subtraction was performed in software before the currents were normalised. Statistical analysis was performed using Student's *t*-test and differences were considered significant when $p < 0.05$.

*Pulse Protocols.* The voltage dependence of activation was studied by measuring the normalised peak currents during 100 ms depolarisations from -120 mV to +30 mV in 5 mV increments. The resulting I-V curve was fit to the equation $I=[1+\exp(-0.03937.z.(V-V1/2)]-1.g.(V-Vr)$ (I, current amplitude; z, apparent gating charge; V test potential; $V_{1/2}$, half maximal voltage; g, factor related to the maximum number of open channels; and Vr, reversal potential). Conductance was determined using G=I/(V-Vr). To study the steady-state fast inactivation, cells were held at conditioning pre-pulse potentials ranging from −120 mV to +30 mV in 5 mV increments from a holding potential of −120 mV and a test pulse at 0 mV for 20 ms. The peak current amplitudes during the subsequent test pulses were normalised to the peak current amplitude during the first test pulse and plotted against the potential of the conditioning pulse. Recovery from fast inactivation was studied by pre-pulsing the cells to 0 mV from a holding potential of −120 mV for 30 ms to fully inactivate channels. The voltage was then returned to the holding potential of −120 mV for variable intervals (every 3 ms from 0 to 39 ms). Finally, the voltage was stepped to 0 mV for 30 ms to test channel availability. The peak current amplitude during the test potentials was plotted as fractional recovery against the recovery period by normalising to the maximum current during the conditioning potentials. The recovery currents were plotted against delta time.

To examine the effects of AEDs, two voltage protocols were used. In the first, the cells were held at -60 mV and 20 millisecond test depolarisations were applied in 10 mV increments, from -80 mV to +60 mV. The cells were then exposed to vehicle control (DMSO), followed by 50 μM CBZ and then 10 μM TTX in the continued presence of 50 μM CBZ and the voltage protocol utilised for each variable. In the second set of experiments, cells were held at -60 mV and 20 millisecond duration test depolarisations applied every 2 seconds in the presence of vehicle. Data was acquired for 3-5 min to establish a stable control baseline current, during which time vehicle was continuously applied. On establishment of a stable current, CBZ (50 μM) or PHT (50 μM) was applied to the cells for 5 min. Following 3-5 min washout of AED, 10 μM TTX was applied for 2 min. Peak currents for individual cells were averaged over 30 s periods

directly before application of AED, following establishment of block in the presence of AED and following establishment of block by TTX.

**RESULTS**

We identified the presence of functional $Na_V$ in primary mouse osteoblasts using RNASeq, immunohistochemistry and patch clamp electrophysiology techniques. RNASeq analysis was used to determine whether voltage-gated sodium channels are expressed by primary mouse osteoblast cultures. Utilizing a threshold of 0.3 FPKM, a number of genes encoding voltage-gated sodium channels (including α and β subunits) were found to be expressed (Table 1). Expression of the genes *Scn2a1* ($Na_V$ 1.2), *Scn3a* ($Na_V$ 1.3), *Scn7a* (also referred to as *Scn6a*, NaG, $Na_X$, $Na_{Vi}2.1$, $Na_V2.1$ or $Na_V2.2$), *Scn1b* ($Na_V\beta1$) and *Scn3b* ($Na_V\beta3$) was revealed using this method. Specific immunofluorescence staining for $Na_V$ (Pan α) was observed (Fig 1), providing further evidence of sodium channel expression in the primary cultured osteoblasts.

The biophysical properties of endogenous inward sodium currents were analyzed in mouse primary calvarial osteoblasts using a high throughput automated planar patch-clamp technology. Specifically, the voltage-dependence of activation, fast-inactivation and recovery from fast inactivation were examined. Eight separate primary calvarial cell digests were utilized: data for CBZ are pooled from 3 digests and for PHT from a further 2 digests; the biophysical data are pooled from 2 digests. Representative current family traces illustrate the robust voltage-activated inward currents elicited in these cells (Fig 2A). Current-voltage (I/V) curves, normalised to the maximum inward current were calculated and as expected for $Na_V$, show a voltage-dependence of activation with the threshold of activation close to -40 mV and the peak current close to 0 mV (Fig 2B). The voltage-dependence of activation and fast-inactivation was examined by converting the peak current versus voltage curves into conductance versus voltage (G–V) and fit to a Boltzmann function (Fig 2C). The half maximal voltage for activation and inactivation was -7.81 ± 0.47 mV and -42.9 ± 0.72 mV, respectively. The slope of the activation and inactivation curves was 7.71 ± 0.38 and 9.30 ± 0.63 (n = 13), respectively. Normalised current as a function of time following an inactivating voltage step was plotted and the curve was fit with a hyperbola as a means to characterise data, for which the recovery constant was 1.59 ± 0.16 (n = 13) (Fig 2D).

External application of CBZ resulted in significant inhibition of current amplitude and this is reflected in the representative raw current traces obtained from a single cell using this voltage protocol (Fig 3A). In the second set of experiments, cells were held at -60 mV and on establishment of a stable baseline current, 50 μM CBZ was applied for 5 minutes. The inset is a representative recording from a single cell showing the time course of block by CBZ, its subsequent wash-off, followed by almost complete block in the presence of TTX confirming presence of $Na_V$ channels. The blocking effect of CBZ was consistent across all cells tested as highlighted by the averaged raw current traces (Fig 3B) as well as the averaged and normalized I/V plots (Fig 3C). CBZ caused a significant inhibition of current amplitude (31.6 ± 5.9 % inhibition, n = 9, $p<0.001$) (Fig 3D), which was partially reversed upon washout (see Fig 3A inset), whereas its vehicle, DMSO, was without effect (data not shown). Furthermore, subsequent application of 10 μM TTX, a

known sodium channel blocker, resulted in almost complete inhibition of the current (89.96 ± 2.14 % inhibition, n = 9, $p<0.00001$) (Fig 3D).

In the next series of experiments the effect of external application of PHT (50 μM) was examined. PHT also inhibited the TTX sensitive current; however, this effect was not reversed upon washout (see Fig 3E inset). Representative raw current traces from a single cell illustrate the degree of block by PHT and TTX (Fig 3E). The inset demonstrates the time course of block by PHT and TTX in a single cell. The averaged raw traces and the normalised I/Vs show the degree of block by PHT across several cells (Fig 3F-G). The percent inhibition by PHT was statistically significant (35.5 ± 6.9 % inhibition, n = 7, $p<0.001$) (Fig. 3H).



**DISCUSSION**

This study characterized the molecular and functional expression of $Na_V$s in mouse primary calvarial osteoblasts and showed they were inhibited by the commonly prescribed AEDs CBZ and PHT. To our knowledge, this is the first study to report inhibitory effects of AEDs CBZ and PHT on $Na_V$ in osteoblastic cells, providing primary evidence for a direct effect on bone cells and, therefore, potentially on bone health. The electrophysiological characteristics of the voltage-gated sodium current in osteoblasts were found to be similar to those of neuronal sodium currents: the native osteoblastic sodium currents here were activated by depolarisations above -40 mV, exhibited steady-state fast inactivation with a V-half value around -43 mV, and were blocked by TTX [32].

Although it has been demonstrated previously that osteoblasts are able to generate APs [20], the role and significance for these APs is not altogether clear. If APs were, for instance, generated during loading or stress detection, or initiate or contribute to signaling during bone remodeling, it is possible that AEDs that interfere with AP firing could increase fracture risk in patients medicated with certain AEDs. This effect could provide a mechanism by which a diverse group of molecules could have a similar, adverse effect on bone.

The genes identified in RNASeq analysis as being expressed by osteoblast cultures encode both the alpha pore forming and beta accessory subunits, indicating that functional $Na_V$s are likely present in mouse osteoblasts. Both α and β subunits have important roles in the structure and function of $Na_V$; the α subunit forms the pore, while associated β subunits (which are also tissue specific), can direct trafficking and also modulate α subunit function [33; 34].We note that cells utilized in the RNASeq were cultured utilizing different media to those utilized in immunocytochemistry and electrophysiology experiments, and therefore it remains possible that other $Na_V$ subtype expression under different media conditions, or at differing times in culture are also present. Identifying functional expression of $Na_V$ and investigating electrophysiological responses of $Na_V$ currents to AEDs was our primary aim, rather than specifically confirming the subtype which the AEDs examined act upon in this study. The results of the RNASeq showed that of the genes encoding α subunits, the most highly expressed was *Scn7a* ($Na_{Vi}2.1$), which despite belonging to the family of voltage-gated sodium channels is a voltage- and TTX-insensitive sodium channel thought to be involved in sodium sensing and contributing to depolarization of the resting membrane potential in neurons [35]. As a channel that is thought to

be $Na^+$ permeant at rest it would exert a permanent depolarizing influence on the osteoblasts. The cellular role and effects of AEDs on $Na_Vi2.1$ are not known, partly due to the difficulty in obtaining functional heterologous expression [36]. As the currents recorded in this experiment were TTX sensitive (to TTX in the micromolar range) the recordings obtained here are not consistent with that of $Na_Vi2.1$ and are therefore more likely attributable to $Na_V$ 1.2 and/or $Na_V$ 1.3 TTX sensitive currents.

A previous study showed that both PHT and CBZ inhibited proliferation of human osteoblast-like cells at therapeutic concentrations, indicating this decrease in proliferation may impair new bone formation [7]. However, electrophysiology was not performed to investigate specific effects at the ion channel level. Altered membrane potential and reduced electrical coupling via gap junctions in the presence of CBZ and PHT [37] have been shown in a previous study of rat primary osteoblasts; however, $Na_V$ were not examined. Further studies are required to examine effects of other AEDs on $Na_V$ as well as other ion channels in osteoblasts, osteocytes, osteoclasts, and in human cells to further explore the effects of AEDs on bone health.

These *in vitro* studies have demonstrated osteoblast ion channels that are sensitive to inhibition by two common AEDs, providing a potential mechanism of increased fracture risk in patients via direct effects of AEDs on osteoblast function.

KEY POINT BOX

- Immunocytochemistry and automated electrophysiology showed functional expression of voltage gated sodium currents in mouse primary osteoblasts
- Carbamazepine and phenytoin resulted in significant inhibition of sodium current amplitude
- The inhibition of sodium currents in osteoblasts by anti-epileptic medications is a potential mechanism for altered bone strength in epilepsy



**Acknowledgement - Funding**

The authors would like to sincerely acknowledge the following organizations for funding received during the development of this study including: the Molly McDonnell Foundation Scholarship (2009), DW Keir Fellowship in Medical Research at The Royal Melbourne Hospital (January 2010- June 2012), University of Melbourne Early Career Researcher (ECR) grant (2010); Brain Foundation Research Grant-in-Aid (2011); The Royal Melbourne Hospital Home Lottery Grants-in-Aid (2012), RACP Servier Barry Young Fellowship in Neuroscience (2012), The Royal Melbourne Hospital Victor Hurley Grants-in-Aid (2013) and MBC Postdoctoral Medical Research Fellowship at The Melbourne Brain Centre RMH (June 2012-2014) (NHMRC Centre for Research Excellence Grant 1001216). Dr. Sandra Petty held the Thwaites Gutch Fellowship at Ormond College Parkville 2011-2015.

**Author Contributions**

S.J.P, J.D.W., and E.J.M. conceived the study; S.J.P., C.J.M., K.L.R., M.T., C.N.P., E.J.M., C.F., E.L.H-Y., T.J.O., J.D.W. and S.P. contributed to project design; S.J.P, C.J.M., M.T., P.K.K., C.N.P. and K.L.R. performed the laboratory experiments; C.J.M, S.J.P and S.P. designed the analysis; C.J.M. performed the analysis. S.J.P, C.J.M and S.P. co-wrote the manuscript. All authors edited and reviewed the manuscript. S.J.P and C.J.M contributed equally as first authors. We acknowledge prior research assistance of Sarah Miller on the AED Osteoblast project.

**Potential Conflicts of Interest**

None of the authors has any conflict of interest to disclose. We confirm that we have read the Journal's position on issues involved in ethical publication and affirm that this report is consistent with those guidelines.

**FIGURE LEGENDS**

**Figure 1. Immunocytochemistry staining of cells from mouse calvarial osteoblast cultures with $Na_V$ (Pan-α) antibody and DAPI nuclear counterstaining.** (**A**) $Na_V$ (Pan alpha) antibody stain. (**B**) DAPI nuclear counterstain of the field shown in A. (**C**) No primary antibody control. (**D**) DAPI counterstain of the field shown in C

**Figure 2. Characterization of sodium currents recorded in mouse primary calvarial osteoblastic cells.** (**A**) Representative current traces obtained from a single cell using a voltage-dependence of activation protocol. (**B**) Normalized current-voltage relationship curve averaged from 13 cells. Inset shows the voltage protocol. (**C**) Voltage-

dependence of normalised peak conductance (□) and steady-state inactivation (○) shown as a function of voltage. Currents were normalized to the maximum peak current. Pulse protocol for steady-state inactivation shown in the inset. For both graphs Boltzmann curves were fit to pooled averages (n = 13 cells) and plotted. (**D**) Recovery of channel availability from fast-inactivation shown as a function of time. A hyperbola was fit to pooled averages and plotted. Schematic of pulse protocol is shown in the inset.

**Figure 3. Inhibitory effects of carbamazepine and phenytoin on voltage-dependent sodium currents recorded in C57BL/6J mouse primary calvarial osteoblasts** (**A**) Representative current traces obtained from a single cell in the presence of vehicle (navy traces), CBZ (50 μM; red traces) or TTX (10 μM; green traces), respectively. Cells were held at -60mV and stepped from -80mV to +60mV for 20 milliseconds every 2 seconds. Scale bars apply to all traces. Representative recording showing peak current plotted against time illustrating the blocking effect of CBZ, washout of CBZ and subsequent block by TTX are shown in the inset. (**B**) Averaged current traces in the presence of vehicle (navy trace), 50 μM CBZ (red trace) or 10 μM TTX (green trace). Cells were held at -60mV and repeatedly stepped to 0mV for 20 milliseconds every 2 seconds (n = 9 cells). (**C**) Normalized average current-voltage relationships in the presence of vehicle (pale blue ○), 50 μM CBZ (red △) and 10 μM TTX (green □). Currents were normalized to the maximum peak current in the presence of vehicle (n = 9 cells). (**D**) Average percent inhibition by 50 μM CBZ (red) and 10 μM TTX (green) (n = 9 cells). (**E**) Representative current traces obtained from a single cell in the presence of vehicle (navy traces), PHT (50 μM; blue traces) or TTX (10 μM; green traces). Scale bars apply to all traces. Same voltage protocol as A. Representative recording showing peak current plotted against time illustrating the blocking effect of PHT, washout of PHT and subsequent block by TTX are shown in the inset. (**F**) Averaged current traces in the presence of vehicle (navy trace), 50 μM PHT (blue trace) or 10 μM TTX (green trace) (n = 7 cells). Same voltage protocol as B. (**G**) Normalized average current-voltage relationships in the presence of vehicle (pale blue ○), 50 μM PHT (blue △) and 10 μM TTX (green □). Currents were normalized to the peak current in the presence of vehicle (n = 7 cells). (**H**) Average percent inhibition by 50 μM PHT (blue) and 10 μM TTX (green) (n = 7 cells). For D and H the peak currents in the presence of CBZ, PHT or TTX were compared to the peak currents in the presence of vehicle. **$p<0.01$, ****$p<0.0001$.

**Table 1. RNAseq results for genes expressed encoding voltage-gated sodium channels (including alpha and beta subunits): FPKM >0.3, and 95% Confidence Intervals.**

REFERENCES

1. Vestergaard P. Epilepsy, osteoporosis and fracture risk - a meta-analysis. *Acta Neurol Scand* 2005;112:277-286.
2. Petty SJ, Paton LM, O'Brien TJ, et al. Effect of antiepileptic medication on bone mineral measures. *Neurology* 2005;65:1358-1365.
3. Andress DL, Ozuna J, Tirschwell D, et al. Antiepileptic drug-induced bone loss in young male patients who have seizures. *Arch Neurol* 2002;59:781-786.
4. Moro-Alvarez MJ, Diaz Curiel M, de la Piedra C, et al. Bone disease induced by phenytoin therapy: clinical and experimental study. *Eur Neurol* 2009;62:219-230.
5. Petty SJ, O'Brien TJ, Wark JD. Anti-epileptic medication and bone health. *Osteoporos Int* 2007;18:129-142.
6. Sander JW. The epidemiology of epilepsy revisited. *Curr Opin Neurol* 2003;16:165-170.
7. Feldkamp J, Becker A, Witte OW, et al. Long-term anticonvulsant therapy leads to low bone mineral density--evidence for direct drug effects of phenytoin and carbamazepine on human osteoblast-like cells. *Exp Clin Endocrinol Diabetes* 2000;108:37-43.
8. Cummings SR, Nevitt MC, Browner WS, et al. Risk factors for hip fracture in white women. Study of Osteoporotic Fractures Research Group. *N Engl J Med* 1995;332:767-773.
9. Fitzpatrick LA. Pathophysiology of bone loss in patients receiving anticonvulsant therapy. *Epilepsy Behav* 2004;5 Suppl 2:S3-15.
10. Sato Y, Kondo I, Ishida S, et al. Decreased bone mass and increased bone turnover with valproate therapy in adults with epilepsy. *Neurology* 2001;57:445-449.
11. Ensrud KE, Walczak TS, Blackwell TL, et al. Antiepileptic drug use and rates of hip bone loss in older men: a prospective study. *Neurology* 2008;71:723-730.
12. Rawlinson SC, Pitsillides AA, Lanyon LE. Involvement of different ion channels in osteoblasts' and osteocytes' early responses to mechanical strain. *Bone* 1996;19:609-614.
13. Zanello LP, Norman AW. Multiple molecular mechanisms of 1 alpha,25(OH)2-vitamin D3 rapid modulation of three ion channel activities in osteoblasts. *Bone* 2003;33:71-79.
14. Black JA, Waxman SG. Sodium channel expression: a dynamic process in neurons and non-neuronal cells. *Dev Neurosci* 1996;18:139-152.
15. Chakkalakal DA. Mechanoelectric Transduction in Bone. *Journal of Materials Research* 1989;4:1034-1046.
16. Pavalko FM, Norvell SM, Burr DB, et al. A model for mechanotransduction in bone cells: the load-bearing mechanosomes. *J Cell Biochem* 2003;88:104-112.
17. Turner CH, Pavalko FM. Mechanotransduction and functional response of the skeleton to physical stress: the mechanisms and mechanics of bone adaptation. *J Orthop Sci* 1998;3:346-355.
18. Sun J, Liu X, Tong J, et al. Fluid shear stress induces calcium transients in osteoblasts through depolarization of osteoblastic membrane. *J Biomech* 2014;47:3903-3908.
19. Chesnoy-Marchais D, Fritsch J. Activation of hyperpolarization and atypical osmosensitivity of a Cl- current in rat osteoblastic cells. *J Membr Biol* 1994;140:173-188.
20. Pangalos M, Bintig W, Schlingmann B, et al. Action potentials in primary osteoblasts and in the MG-63 osteoblast-like cell line. *J Bioenerg Biomembr* 2011;43:311-322.

21. Zanello LP, Norman A. 1alpha,25(OH)2 vitamin D3 actions on ion channels in osteoblasts. *Steroids* 2006;71:291-297.
22. Hodgkin AL, Huxley AF. A quantitative description of membrane current and its application to conduction and excitation in nerve. *J Physiol* 1952;117:500-544.
23. Black JA, Waxman SG. Noncanonical roles of voltage-gated sodium channels. *Neuron* 2013;80:280-291.
24. Vestergaard P, Rejnmark L, Mosekilde L. Fracture risk associated with use of antiepileptic drugs. *Epilepsia* 2004;45:1330-1337.
25. Lee RH, Lyles KW, Colon-Emeric C. A review of the effect of anticonvulsant medications on bone mineral density and fracture risk. *Am J Geriatr Pharmacother* 2010;8:34-46.
26. Pack AM. Treatment of epilepsy to optimize bone health. *Curr Treat Options Neurol* 2011;13:346-354.
27. Pagel CN, Song SJ, Loh LH, et al. Thrombin-stimulated growth factor and cytokine expression in osteoblasts is mediated by protease-activated receptor-1 and prostanoids. *Bone* 2009;44:813-821.
28. NHMRC. Australian code for the care and use of animals for scientific purposes. In Editor (Ed)^(Eds) Book Australian code for the care and use of animals for scientific purposes., Commonwealth of Australia: Canberra: ; 2013.
29. Trapnell C, Salzberg SL. How to map billions of short reads onto genomes. *Nat Biotechnol* 2009;27:455-457.
30. Trapnell C, Williams BA, Pertea G, et al. Transcript assembly and quantification by RNA-Seq reveals unannotated transcripts and isoform switching during cell differentiation. *Nat Biotechnol* 2010;28:511-515.
31. Ramskold D, Wang ET, Burge CB, et al. An abundance of ubiquitously expressed genes revealed by tissue transcriptome sequence data. *PLoS Comput Biol* 2009;5:e1000598.
32. Waxman SG. Sodium channels, the electrogenisome and the electrogenistat: lessons and questions from the clinic. *J Physiol* 2012;590:2601-2612.
33. Patino GA, Isom LL. Electrophysiology and beyond: multiple roles of Na+ channel beta subunits in development and disease. *Neurosci Lett* 2010;486:53-59.
34. Namadurai S, Yereddi NR, Cusdin FS, et al. A new look at sodium channel beta subunits. *Open Biology* 2015;5.
35. Ke CB, He WS, Li CJ, et al. Enhanced SCN7A/Nax expression contributes to bone cancer pain by increasing excitability of neurons in dorsal root ganglion. *Neuroscience* 2012;227:80-89.
36. Savio-Galimberti E, Gollob MH, Darbar D. Voltage-gated sodium channels: biophysics, pharmacology, and related channelopathies. *Frontiers in Pharmacology* 2012;3.
37. Schirrmacher K, Brummer F, Dusing R, et al. Dye and electric coupling between osteoblast-like cells in culture. *Calcif Tissue Int* 1993;53:53-60.

**Table 1. RNAseq results for genes expressed encoding voltage-gated sodium channels (including alpha and beta subunits): FPKM >0.3, and 95% Confidence Intervals.**

| Gene symbol | Gene Name; synonym | FPKM | 95% CI low | 95% CI high |
|---|---|---|---|---|
| Scn2a1 | sodium channel, voltage gated, type II alpha subunit; $Na_V1.2$ | 1.4821 | 0.9256 | 2.0404 |
| Scn3a | sodium channel, voltage gated, type III alpha subunit; $Na_V1.3$ | 0.5222 | 0.2786 | 0.7631 |
| Scn7a | sodium channel, voltage gated, type VII alpha subunit; $Na_{Vi}2.1$ | 3.6029 | 2.4555 | 4.7530 |
| Scn1b | sodium channel, voltage gated, type I beta subunit | 34.8005 | 22.9675 | 45.8203 |
| Scn3b | sodium channel, voltage gated, type III beta subunit | 2.1051 | 1.2063 | 3.0036 |

**KEY:**

**FPKM** fragments per kilobase of exon per million fragments mapped

**CI** confidence interval

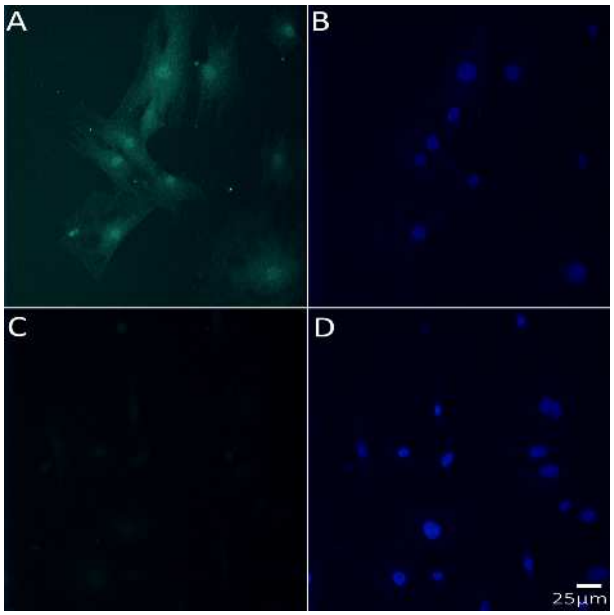


epi_13474_f1.tif

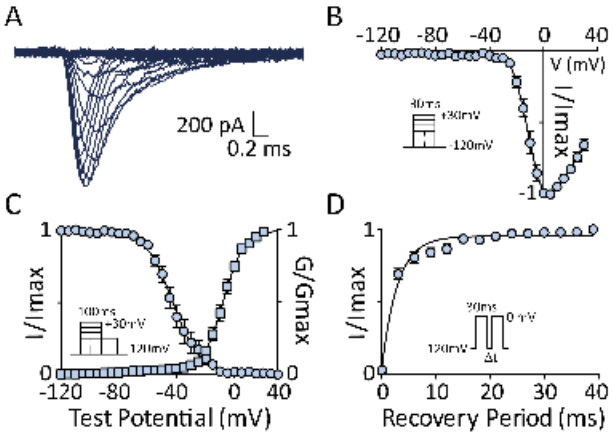


epi_13474_f2.tif

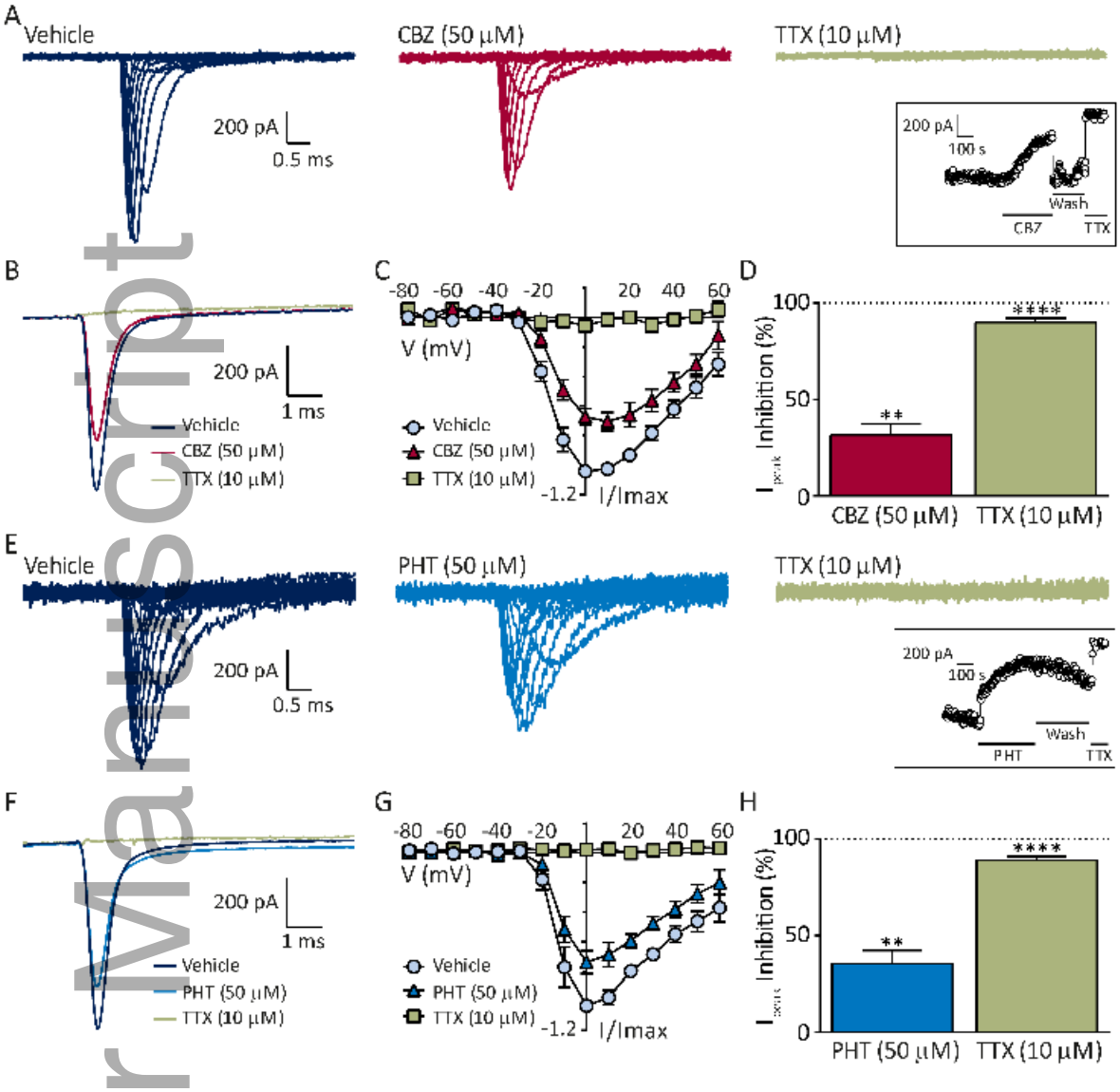


epi_13474_f3.tif